Received: 6 September 2022 | Accepted: 9 November 2022

DOI: 10.1002/pamm.202200008

A magneto-mechanically coupled material model for magnetic sensor investigation

Christian Dorn[1,*] and **Stephan Wulfinghoff**[1,**]

[1] Institute for Materials Science – Computational Materials Science, Kiel University, 24143 Kiel, Germany

We consider coupled micro-magneto-mechanics with the aim to understand the processes which underpin magnetic noise in composite magnetoelectric sensors. We formulate a material model within the generalized standard material framework. This approach ensures thermodynamic consistency. Using our material model, we study the interaction of domain walls with two types of defects: geometrical defects and eigenstrains. We discuss the interaction and underlying effects in detail.

1 Introduction

Measuring small magnetic fields (e.g. of heart and brain) requires sensors with high sensitivity and low noise. Typically SQUID (superconducting quantum interference device) or OPM (optically pumped magnetometer) sensors are utilized for these use cases. However, these magnetometers exhibit high complexity and operating expenses. Hence there is a demand for alternative sensor concepts (cheap, easy-to-use) [10]. Composite magnetoelectric thin film sensors are one example for an alternative concept. This sensor concept is based on the interaction of multiple coupled fields in the involved magnetostrictive and piezoelectric thin film materials. The route starts with magnetic signals in the magnetostrictive material and proceeds via mechanics and surface coupling to electric signals in the piezoelectric material.

Currently, one limiting factor for sensor performance is magnetic noise. This type of noise is caused by detrimental magnetic processes that disturb the signal [2, 5, 13]. In particular these processes are intrinsic to the magneto-mechanical material. Thus, we concentrate on the magneto-mechanical part and omit the piezoelectric part of the sensor principle for our investigation. In this work we focus on the interaction of domain walls with various types of defects (as one of the aforementioned detrimental magnetic processes).

2 Problem setting and kinematics

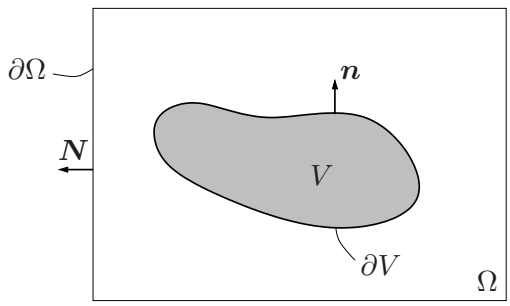

Fig. 1: Free space Ω with embedded material volume V

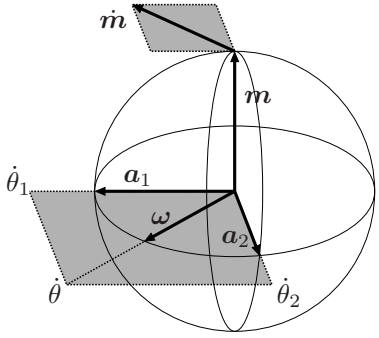

Fig. 2: Kinematics of magnetization $\boldsymbol{m}$

The coupled micro-magneto-mechanical problem is posed in the free space box $\Omega \subset \mathbb{R}^3$ in which the material volume $V \subset \Omega$ is embedded, see Fig. 1. Material volume and free space box have the external normals $\boldsymbol{n}$ resp. $\boldsymbol{N}$. We define time to be in the range $[0, T] \subset \mathbb{R}$. Three field quantities characterize the coupled problem: displacement $\boldsymbol{u}$, magnetization $\boldsymbol{m}$ and scalar magnetic potential φ

$$\boldsymbol{u} : V \times [0,T] \to \mathbb{R}^3, \qquad \boldsymbol{m} : V \times [0,T] \to \mathcal{S}^2, \qquad \varphi : \Omega \times [0,T] \to \mathbb{R}, \tag{1}$$

where $\mathcal{S}^2$ denotes unit sphere in $\mathbb{R}^3$. We formulate the kinematics of the mechanical sub-problem in the small strain setting. Hence, we employ the strain tensor $\boldsymbol{\varepsilon}$

$$\boldsymbol{\varepsilon} = \frac{1}{2}\left(\nabla \boldsymbol{u} + (\nabla \boldsymbol{u})^{\top}\right) \tag{2}$$

* Corresponding author: e-mail cdo@tf.uni-kiel.de, phone +49 431 880 6317, fax +49 431 880 6246
** e-mail swu@tf.uni-kiel.de phone +49 431 880 6243, fax +49 431 880 6246

to describe deformation. Further, we assume an additive decomposition of strain

$$\boldsymbol{\varepsilon} = \boldsymbol{\varepsilon}^{\mathrm{e}} + \boldsymbol{\varepsilon}^{\mathrm{m}} + \boldsymbol{\varepsilon}^{\star} \tag{3}$$

into an elastic part $\boldsymbol{\varepsilon}^{\mathrm{e}}$, a magnetostrictive strain $\boldsymbol{\varepsilon}^{\mathrm{m}}$ and an eigenstrain contribution $\boldsymbol{\varepsilon}^{\star}$. As for the kinematics of the magnetic sub-problem, the magnetization $\boldsymbol{m}$ is restricted to the unit sphere (i.e. $\|\boldsymbol{m}\| = 1$). Hence we express the evolution of magnetization $\dot{\boldsymbol{m}}$ (and the accompanying vectors $\dot{\boldsymbol{a}}_1, \dot{\boldsymbol{a}}_2$) as follows

$$\{\dot{\boldsymbol{a}}_1, \dot{\boldsymbol{a}}_2, \dot{\boldsymbol{m}}\} = \dot{\theta}\boldsymbol{\omega} \times \{\boldsymbol{a}_1, \boldsymbol{a}_2, \boldsymbol{m}\}, \qquad \dot{\theta}\boldsymbol{\omega} = \dot{\theta}_1 \boldsymbol{a}_1 + \dot{\theta}_2 \boldsymbol{a}_2, \tag{4}$$

cf. Fig. 2. We adopt the exponential map algorithm to implement this kinematic constraint, cf. [6, 9, 11, 12].

3 Material modeling

We formulate the material model within the generalized standard material (GSM) framework [4,8]. Two contributions describe the material behavior: the free energy $\Psi = \Psi_{\mathrm{ex}} + \Psi_{\mathrm{a}} + \Psi_{\mathrm{d}} + \Psi_{\mathrm{z}} + \Psi_{\mathrm{el}}$ and dissipation potential Φ, see Tab. 1. The free energy reflects conservative material behavior while the dissipation potential Φ represents dissipative material behavior. As a result of the GSM approach, the second law of thermodynamics is automatically fulfilled.

We summarized the free energy rate $\dot{\Psi}$ and the dissipation potential Φ in the time continuous rate potential $\Pi = \dot{\Psi} + \Phi$. Time discretization yields the time discrete incremental potential Π_Δ which we aim to optimize. From the potential optimization

$$\Pi_\Delta \to \underset{\boldsymbol{u},\boldsymbol{m},\varphi}{\mathrm{stat}} \qquad \text{with} \qquad \|\boldsymbol{m}\| = 1 \tag{5}$$

we obtain three stationary points which are the weak forms of linear momentum balance, Landau-Lifschitz-Gilbert equation [3] and Gauss' law. We use these stationary points as residuals for global Newton-Raphson scheme.

Table 1: Contributions to the GSM formulation

exchange energy	$\Psi_{\mathrm{ex}}(\nabla\boldsymbol{m}) = \int_V A\,\|\nabla\boldsymbol{m}\|^2\,\mathrm{d}V$
anisotropy energy	$\Psi_{\mathrm{a}}(\boldsymbol{m}) = \int_V K_1\big(1-(\boldsymbol{m}\cdot\boldsymbol{e}_{\mathrm{a}})^2\big)\,\mathrm{d}V$
demagnetizing energy	$\Psi_{\mathrm{d}}(\boldsymbol{m},\nabla\varphi) = \int_V \mu_0\nabla\varphi\cdot M_{\mathrm{s}}\boldsymbol{m}\,\mathrm{d}V - \frac{1}{2}\int_\Omega \mu_0\|\nabla\varphi\|^2\,\mathrm{d}V$ with demagnetizing field $\boldsymbol{H}_{\mathrm{d}} = -\nabla\varphi$
Zeeman energy	$\Psi_{\mathrm{z}}(\boldsymbol{m}) = \int_V -\mu_0 M_{\mathrm{s}}\boldsymbol{m}\cdot\boldsymbol{H}'\,\mathrm{d}V$ with externally applied field $\boldsymbol{H}'$
elastic energy	$\Psi_{\mathrm{el}}(\boldsymbol{\varepsilon},\boldsymbol{m}) = \int_V \frac{1}{2}\,\boldsymbol{\varepsilon}^{\mathrm{e}} : \mathbb{C} : \boldsymbol{\varepsilon}^{\mathrm{e}}\,\mathrm{d}V$ with $\boldsymbol{\varepsilon}^{\mathrm{m}} = \frac{3}{2}\lambda_{\mathrm{s}}\left(\boldsymbol{m}\otimes\boldsymbol{m} - \frac{1}{3}\boldsymbol{I}\right)$
dissipation potential	$\Phi(\dot{\boldsymbol{m}}) = \int_V \frac{\eta}{2}\dot{\boldsymbol{m}}\cdot\dot{\boldsymbol{m}}\,\mathrm{d}V$

4 Numerical experiments

4.1 Implementation

For the solution of the micro-magneto-mechanical problem we use the finite element method. Specifically we use ParFEAP 8.6.1j (MPI-parallel version of FEAP [14]) which is supported by PETSc 3.13.2 [1]. For spatial discretization we employ tetrahedral elements and linear shape functions. For time derivatives we adopt a finite difference scheme. In our implementation there are six degrees of freedom (dof) per node: displacement (3 dof), scalar magnetic potential (1 dof) and magnetization (2 dof).

4.2 Material parameters and problem specification

In the following numerical examples we consider a stack of free space, magneto-mechanical film, mechanical substrate and free space, see Fig. 3. The (estimated) material parameters of magnetic material (FeCoSiB) and substrate are given in Tab. 2. We use periodic boundary conditions in $\boldsymbol{e}_1$- and $\boldsymbol{e}_2$-direction to obtain results without closure domains and effectively represent an infinitely extended composite. To implement the periodic boundary conditions, we adapt the mesh files such that the periodically repeated nodes share the same node number, cf. [7]. We choose the pattern shown in Fig. 4 to prescribe the

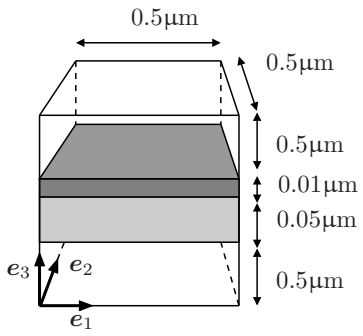

Fig. 3: *Free space – film – substrate – free space* stack, periodic boundary conditions in e_1- and e_2-direction

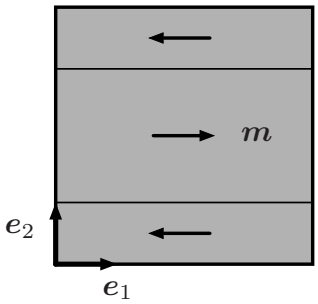

Fig. 4: Initialization of magnetization $m(x, 0)$ in magneto-mechanical film (sketch)

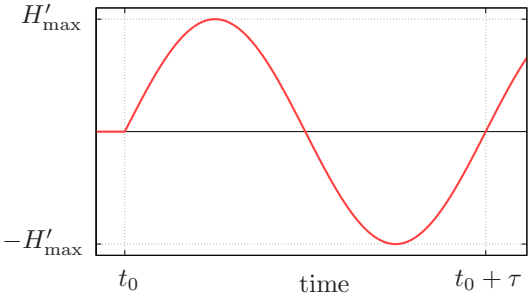

Fig. 5: Applied field $\boldsymbol{H}' = H'(t)\boldsymbol{e}_1$ with $t_0 = 10^{-9}$ s, $\tau = 3 \cdot 10^{-7}$ s

initial magnetization $\boldsymbol{m}(\boldsymbol{x}, 0)$. This pattern is compatible with the periodic boundary conditions and affords us two easily controllable domain walls. We need the latter to investigate the interaction of domain walls and defects. To put the domain walls in motion we exert a sinusoidal applied field $\boldsymbol{H}' = H'(t)\boldsymbol{e}_1$, see Fig. 5. This type of applied field yields a reciprocating domain wall motion and allows multiple interactions with defects. We define the onset of loading at t_0 to afford the system an initial relaxation time in which it assumes an equilibrium state.

Table 2: Estimated material parameters

		FeCoSiB	substrate
A	exchange constant	$1.5 \cdot 10^{-11}\ \frac{\mathrm{J}}{\mathrm{m}}$	–
M_s	spontaneous magnetization	$1.5 \cdot 10^{6}\ \frac{\mathrm{A}}{\mathrm{m}}$	–
K_1	anisotropy constant	$3 \cdot 10^{2}\ \frac{\mathrm{J}}{\mathrm{m}^3}$	–
$\boldsymbol{e}_\mathrm{a}$	easy axis	$\boldsymbol{e}_1$	–
η	viscosity parameter	$1 \cdot 10^{-5}\ \frac{\mathrm{J \cdot s}}{\mathrm{m}^3}$	–
λ_s	saturation magnetostriction	$30 \cdot 10^{-6}$	–
λ	first Lamé parameter	172 GPa	150 GPa
μ	second Lamé parameter	54 GPa	50 GPa

4.3 Domain wall interaction with geometrical defects

To study the interaction of domain walls with defects we need to introduce defects into the magnetic film. As prototypical defects we consider two cylindrical holes with radius 10 nm that penetrate entire thickness of the film, cf. Fig. 6. The interaction between domain walls and defects is attractive since it is energetically favorable for domain walls to attach to the defects (reduces e.g. exchange energy). For the applied field magnitude we choose $H'_{\max} = 1 \cdot 10^{-2}\,\mathrm{A/\mu m}$.

In Fig. 6 we display a time series of the two prescribed domain walls interacting with the defects, driven by the applied field. On the left of Fig. 6 we observe that the upper domain wall leaps forward and attaches to defect due to attractive interaction. In the center of Fig. 6 both domain walls are attached to defects and resist the applied field. We observe domain wall curvature in the vicinity of the holes. On the right of Fig. 6 the upper domain wall has overcome the defect due to sufficiently large applied field ($\|\boldsymbol{H}'\| \approx 9 \cdot 10^{-3}\,\mathrm{A/\mu m}$).

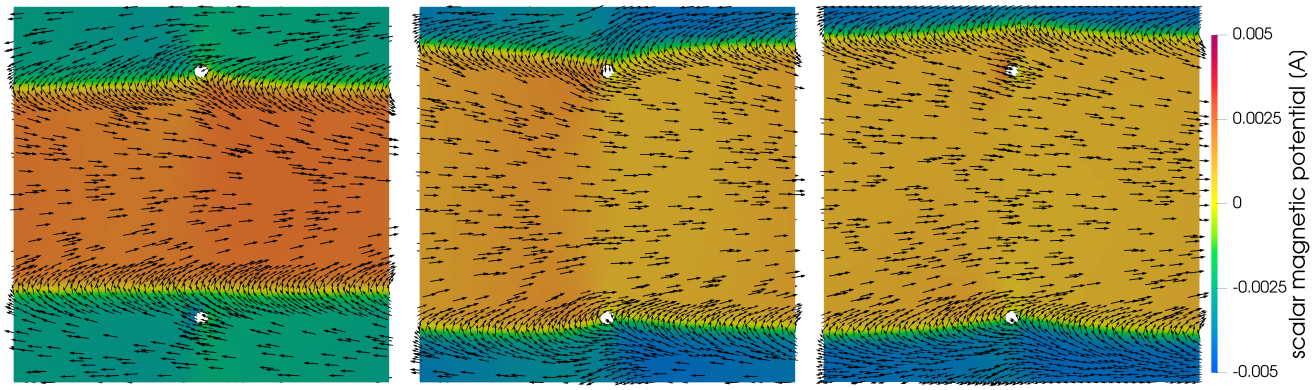

Fig. 6: Time series: interaction of domain walls with cylindrical holes, time points from left to right: $7.6 \cdot 10^{-9}$ s, $5.4 \cdot 10^{-8}$ s, $5.7 \cdot 10^{-8}$ s, displayed: scalar magnetic potential φ and magnetization vectors $\boldsymbol{m}$

4.4 Domain wall interaction with eigenstrain

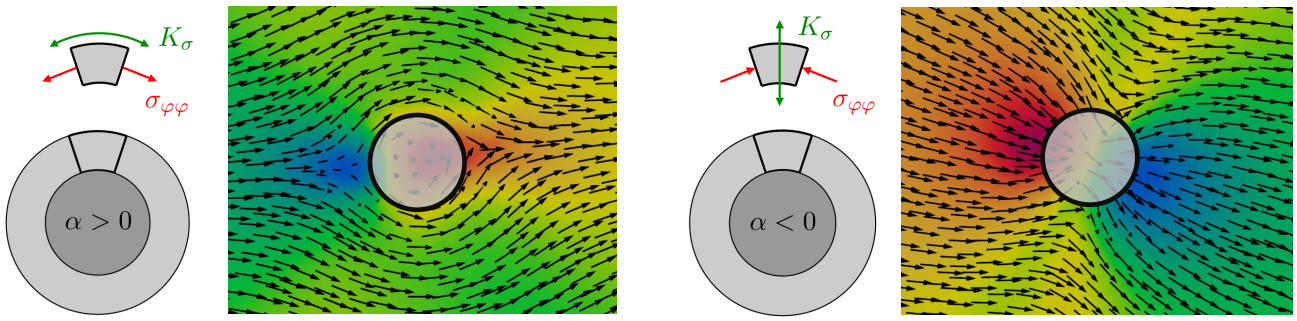

Fig. 7: Left: expansive eigenstrain $\alpha > 0$ yields circumferential tensile stress $\sigma_{\varphi\varphi}$ and circumferential stress-induced anisotropy K_σ, right: contracting eigenstrain $\alpha < 0$ yields circumferential compressive stress $\sigma_{\varphi\varphi}$ and radial stress-induced anisotropy K_σ

Besides geometrical defects we are also interested in the interaction of domain walls with local eigenstrains. To investigate this type of interaction we prescribe an eigenstrain $\boldsymbol{\varepsilon}^\star = \alpha \boldsymbol{I}$ in a spherical volume with radius $5\,\mathrm{nm}$ in the magneto-mechanical film. In the expansive case ($\alpha > 0$) we obtain circumferential tensile stresses $\sigma_{\varphi\varphi}$ around the eigenstrains. These stresses result in a circumferential stress-induced anisotropy K_σ, see Fig. 7 (left). For the contracting case ($\alpha < 0$) we obtain circumferential compressive stresses $\sigma_{\varphi\varphi}$ around the eigenstrains. The stress-induced anisotropy K_σ is aligned in radial direction for this case, see Fig. 7 (right).

The placement of the *eigenstrain spheres* is the same as the placement of the cylindrical holes in section 4.3. In $\boldsymbol{e}_3$-direction the *eigenstrain spheres* are located in the center of the film thickness. For the applied field magnitude we choose in this case $H'_{\max} = 2 \cdot 10^{-2} \, \frac{\mathrm{A}}{\mu\mathrm{m}}$.

In Fig. 8 we show a time series of the two domain walls interacting with expansive eigenstrains ($\alpha = 0.5$), driven by the applied field. The character of the interaction is similar to Fig. 6, i.e. attractive interaction. The applied field to overcome the defect is similar to section 4.3 as well ($\|\boldsymbol{H}'\| \approx 8.9 \cdot 10^{-3}\,\mathrm{A}/\mu\mathrm{m}$). We presume that the attractive interaction occurs because the circumferential anisotropy fits well into the structure of the domain walls.

The time series for the contracting eigenstrain ($\alpha = -1$) is displayed in Fig. 9. On the left of Fig. 9 the domain walls resist attaching to the eigenstrain volumes due to repulsive interaction. Even with larger applied field the domain walls still resist the interaction with the eigenstrain volumes, see Fig. 9 (center). The curvature of the domain walls is larger than in all previous examples. However, with sufficiently large applied field ($\|\boldsymbol{H}'\| \approx 9.7 \cdot 10^{-3}\,\mathrm{A}/\mu\mathrm{m}$) the domain wall overcomes this defect as well, see Fig. 9 (right). We suppose that the repulsive interaction is again due to the stress-induced anisotropy. Albeit in this case, the radial anisotropy of the contracting eigenstrain does not suit the domain wall structure.

Finally we must make one last remark. The eigenstrains (and corresponding stresses) considered here are rather large. We found that strains in such large orders of magnitude were required to achieve an influence of eigenstrain on domain wall motion. The following two reasons appear plausible. Firstly, the coupling between mechanics and magnetics by virtue of the magnetostriction constant λ_s is weak. Hence, large strain is required to compensate. Secondly, the volume in which the eigenstrain is active is very small. Thus, the volume in which mechanics can effectively influence magnetics is very small.

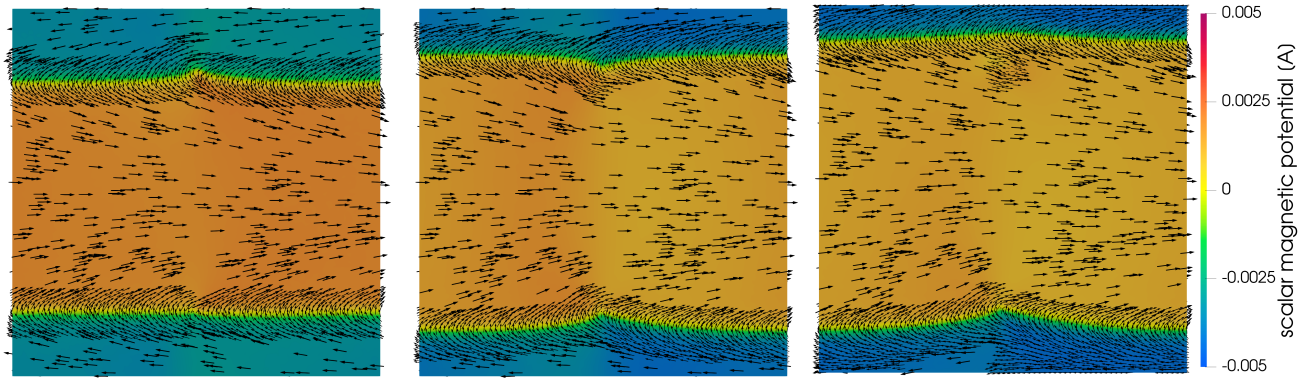

Fig. 8: Time series: interaction of domain walls with expansive eigenstrain ($\alpha = 0.5$), time points from left to right: $9 \cdot 10^{-9}$ s, $2.3 \cdot 10^{-8}$ s, $2.5 \cdot 10^{-8}$ s, displayed: scalar magnetic potential φ and magnetization vectors $\boldsymbol{m}$

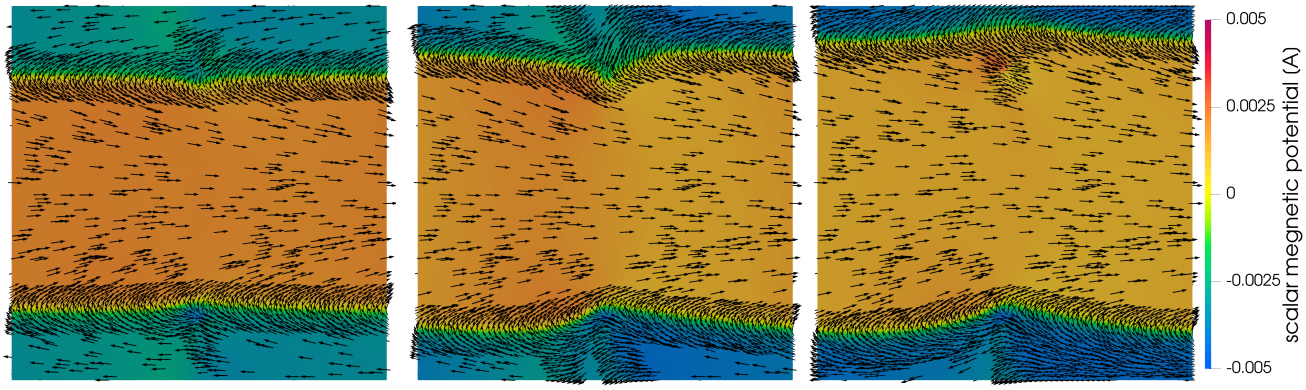

Fig. 9: Time series: interaction of domain walls with contracting eigenstrain ($\alpha = -1$), time points from left to right: $1.2 \cdot 10^{-8}$ s, $2.5 \cdot 10^{-8}$ s, $2.7 \cdot 10^{-8}$ s, displayed: scalar magnetic potential φ and magnetization vectors $\boldsymbol{m}$

5 Summary and outlook

With the present work we showcased our micro-magneto-mechanically coupled material model. The model formulation within the GSM framework ensures thermodynamic consistency. For the unit sphere constraint of the magnetization we apply the exponential map algorithm. The focus of the present work was the investigation of interaction between domain walls and defects. In two numerical examples we investigated the interaction of domain walls with geometrical defects as well as local eigenstrains. In particular we found that the character of the interaction with eigenstrains depends on the sign of latter.

To gain a deeper understanding of the domain wall interaction with eigenstrains, we intend to investigate further examples in the future (different geometries and eigenstrain configurations). Moreover, we strive to compute noise spectra for the presented interactions types.

Acknowledgements This research is funded by the Deutsche Forschungsgemeinschaft (DFG, German Research Foundation) – Projektnummer 286471992 within CRC 1261. Open access funding enabled and organized by Projekt DEAL.

References

[1] Satish Balay, William D. Gropp, Lois C. McInnes, and Barry F. Smith. Efficient management of parallelism in object oriented numerical software libraries. In Erlend Arge, Are M. Bruaset, and Hans P. Langtangen, editors, *Modern Software Tools in Scientific Computing*, pages 163–202. Birkhäuser Press, 1997.

[2] Heinz Bittel. Noise of ferromagnetic materials. *IEEE Transactions on Magnetics*, 5(3):359–365, 1969.

[3] Thomas L. Gilbert. A phenomenological theory of damping in ferromagnetic materials. *IEEE transactions on magnetics*, 40(6):3443–3449, 2004.

[4] Bernard Halphen and Quoc S. Nguyen. Generalized standard materials. *Journal de Mécanique*, 14:39–63, 1975.

[5] Snorri Ingvarsson, Gang Xiao, Stuart S. P. Parkin, William J. Gallagher, Geoffrey Grinstein, and Roger H. Koch. Low-frequency magnetic noise in micron-scale magnetic tunnel junctions. *Physical review letters*, 85(15):3289, 2000.

[6] Debra Lewis and Nilima Nigam. Geometric integration on spheres and some interesting applications. *Journal of Computational and Applied Mathematics*, 151(1):141–170, 2003.
[7] Christian Miehe. Strain-driven homogenization of inelastic microstructures and composites based on an incremental variational formulation. *International Journal for numerical methods in engineering*, 55(11):1285–1322, 2002.
[8] Christian Miehe. A multi-field incremental variational framework for gradient-extended standard dissipative solids. *Journal of the Mechanics and Physics of Solids*, 59(4):898–923, 2011.
[9] Christian Miehe and Gautam Ethiraj. A geometrically consistent incremental variational formulation for phase field models in micromagnetics. *Computer methods in applied mechanics and engineering*, 245:331–347, 2012.
[10] Volker Röbisch, Sebastian Salzer, Necdet O. Urs, Jens Reermann, Erdem Yarar, André Piorra, Christine Kirchhof, Enno Lage, Michael Höft, Gerhard U. Schmidt, Reinhard Knöchel, Jeffrey McCord, Eckhard Quandt, and Dirk Meyners. Pushing the detection limit of thin film magnetoelectric heterostructures. *Journal of Materials Research*, 32(6):1009–1019, 2017.
[11] Juan C. Simo and David D. Fox. On a stress resultant geometrically exact shell model. part i: Formulation and optimal parametrization. *Computer Methods in Applied Mechanics and Engineering*, 72(3):267–304, 1989.
[12] Juan C. Simo, David D. Fox, and Mustapha S. Rifai. On a stress resultant geometrically exact shell model. part iii: Computational aspects of the nonlinear theory. *Computer Methods in Applied Mechanics and Engineering*, 79(1):21–70, 1990.
[13] Djordje Spasojević, Srdjan Bukvić, Sava Milošević, and Harry E. Stanley. Barkhausen noise: Elementary signals, power laws, and scaling relations. *Physical Review E*, 54(3):2531, 1996.
[14] Robert L. Taylor. FEAP - finite element analysis program. http://projects.ce.berkeley.edu/feap/, 2020.